Hydrology and
Earth System
Sciences

Open Access

Supplement of

Adaptation of root zone storage capacity to climate change and its effects on future streamflow in Alpine catchments: towards non-stationary model parameters

Magali Ponds et al.

Correspondence to: Magali Ponds (magali.ponds@vub.be)

5 S1 Model Description

Below the model schematic (Figure S1) and relevant equations (Table S1) are shown. The model considers four hydrological response units (HRUs): bare rock, forested hillslope, grassland hillslope and riparian zone. In each timestep, all units are first run separately. Afterward, the total runoff is generated as the weighted sum of the runoffs of the individual units. The model includes the storage components of interception, unsaturated root zone and a fast and slow storage component, i.e.
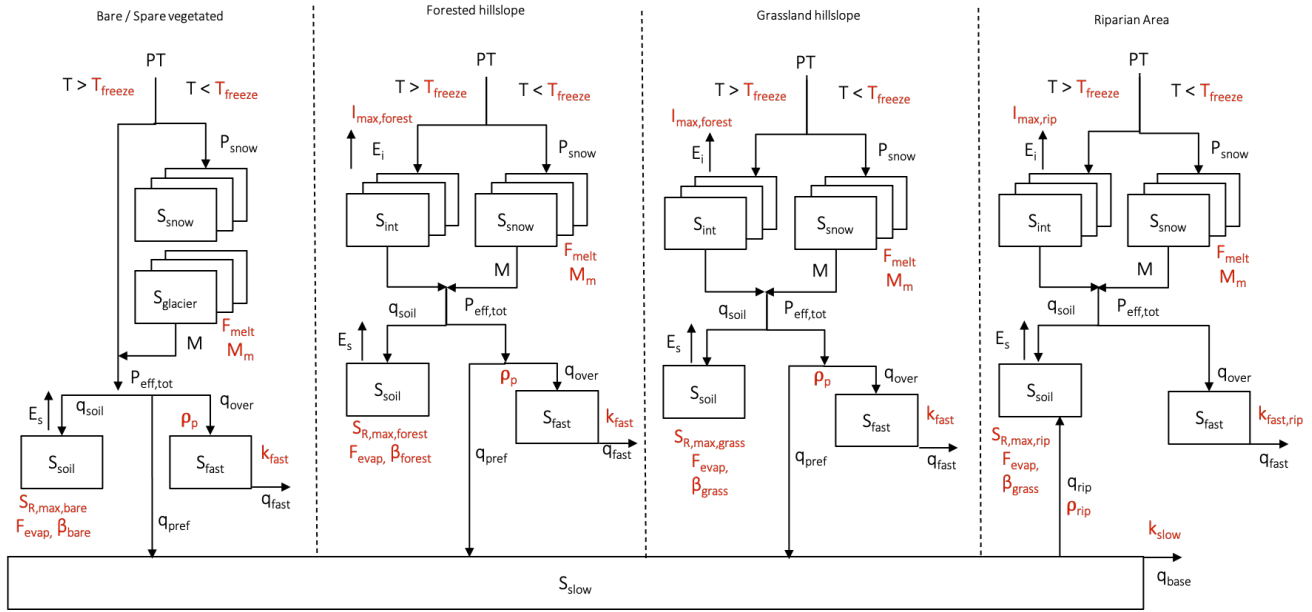10 groundwater.

Fig. S 1. Schematic representation of model structure per precipitation zone. The model is distributed with regard to four Hydrological Response Units, based on topography. Boxes represent states, black arrows are fluxes and parameters are indicated in red

Tab. S 1. List of equations used in the hydrological model. An more extensive description can be found in Hanus (2020)

Reservoir	Water balance Equation	Constitutive functions
Interception	$\frac{dS_{int}}{dt} = P_{rain} - E_{int} - P_{eff}$	$P_{eff} = max(S_{int} - I_{max}, 0)$
		$E_{int} = min(0.5 \cdot E_{pot}, S_{int})$
Snow	$\frac{dS_{snow}}{dt} = P_{snow} - M_{snow}$	$M = F_{melt} \cdot M_M \left(\frac{T - T_{tresh}}{M_M} + ln \left(1 + exp \left(-\frac{T - T_{tresh}}{M_M} \right) \right) \right)$
		$M_{snow} = min(M, S_{snow})$
		$M_{glacier} = M$
		$M_{tot} = M_{snow} \cdot (1 - A_{gl}) + M_{glacier} + A_{gl}$
		$P_{eff,tot} = \sum_{i=1}^{Elevations} P_{eff} + \sum_{i=1}^{Elevations} M_{tot}$
Unsaturated Zone	$\frac{dS_{soil}}{dt} = P_e - E_{soil} - R$	$q_{soil,rip} = P_{eff} + Q_{rip} - R$
	$\frac{dS_{soil,rip}}{dt} = P_e Q_{rip} - E_{soil} - R$	$q_{soil} = P_{eff} + Q_{rip} - R$
		$S_{R,m} = (1 + \beta) S_{R,max} \left(1 - \left(1 - \frac{S_R}{S_{R,max}} \right)^{1/(1+\beta)} \right)$
		$R = P_{eff} - S_{R,max} + S_R + S_{R,max} \cdot \left(1 - \frac{P_{eff} + S_{R,m}}{(1+\beta) S_{R,max}} \beta \right) S_{R,max}^{1+\beta}$
		$Perc = Perc_{max} \frac{S_R}{S_{R,max}}$
		$E_{soil} = (E_{pot} - E_{int}) \cdot min \left(\frac{S_{Soil}}{S_{soil,max} \cdot F_{evap}}, 1 \right)$
		$S_{soil} = S_{Soil} + P_{eff} - E_{Soil} - R$
		$S_{soil,rip} = S_{Soil} + P_{eff} - E_{soil} - R$
Fast Reservoir	$\frac{dS_{fast}}{dt} = q_{overland} - q_{fast}$	$q_{overland} = (P_{eff,tot} - q_{soil}) \cdot \rho_p$
		$q_{overland,rip} = P_{eff,tot} + q_{rip} - q_{soil,rip}$
		$q_{fast} = k_{fast} \cdot S_{fast}$
Slow reservoir	$\frac{dS_{slow}}{dt} = \sum_{i=i}^{HRU} q_{pref} - q_{slow}$	$q_{pref} = (P_{eff,tot} - q_{soil}) \cdot (1 - \rho_p) + R$
		$q_{slow} = k_{slow} \cdot S_{slow}$

S2   Derivation of S_R

As the interception storage capacity (I_{max}) of the interception storage (S_I) is unknown, a random sample of 300 a-priori constrained I_{max} values is used. Through iterative implementation of different I_{max} values, it is observed that a set of 300 values serves as a reliable threshold for achieving a stable range in effective precipitation (P_E) values and resultant root zone storage deficits ($S_{r,D}$). Figure S2 shows the dependency of different I_{max} values on the found S_R parameter ranges for forest and grass respectively. As can be seen, S_R ranges change when using less than 300 I_{max} values, but remain relatively stable when using more than 300 values. Hence, we have decided to use 300 different I_{max} as a threshold for a stable parameter range in S_R.
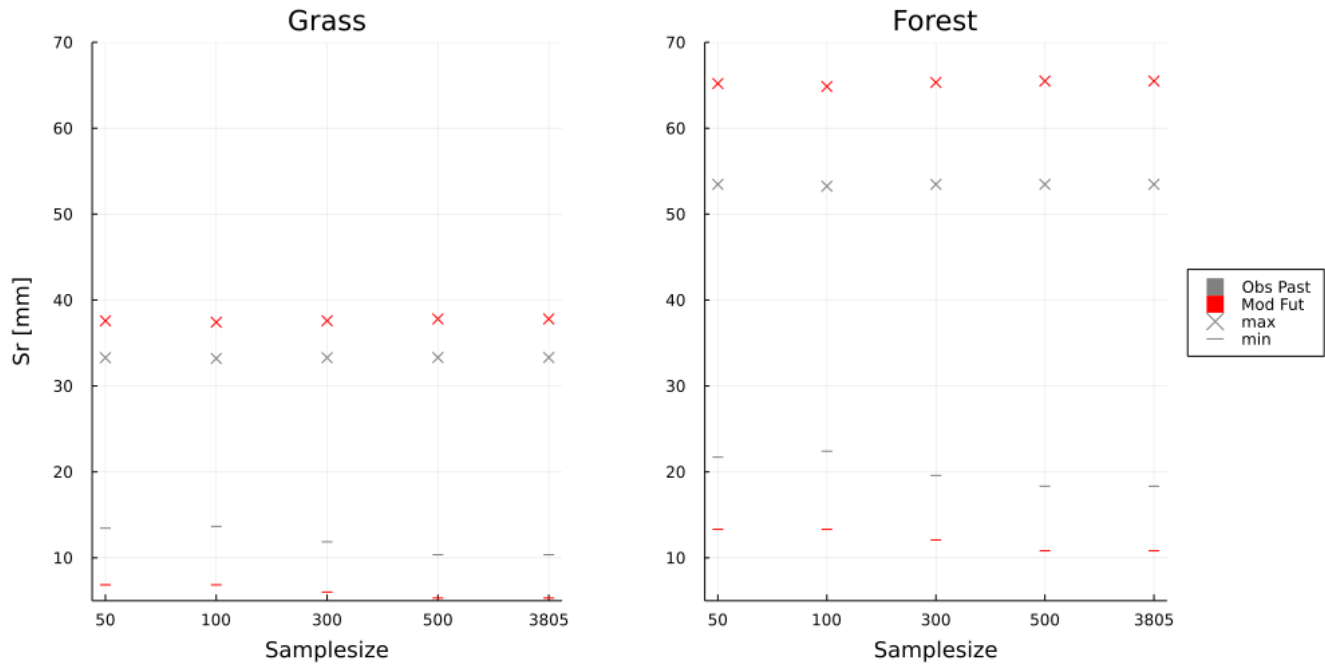

Fig. S 2. Sensitivity analysis of number of I_{max} samples used on the found spread in water balance estimates of S_R
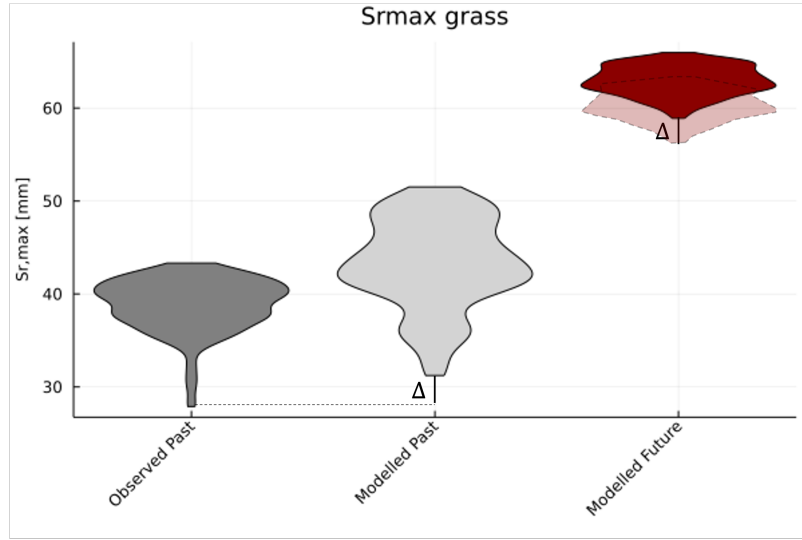
S3 Bias correction climate model

Fig. S 3. Correction for potential climate biases in modelled S_r parameter ranges

The use of climate model data involves uncertainties and potential biases. To limit this, an ensemble of regional climate
model simulations has been deployed. However, a formal correction of climate model data has not been applied, as it
might alter the relations between climate variables (Ehret et al., 2012). Instead, to account for potential biases in the used
climate models, a climate correction has been performed as is proposed in the work of Bouaziz et al. (2021) and shown in
Equation 1 & Figure S3. Here, the bias is defined as the difference in S_r estimates derived from observed and simulated
climate data. It should be noted that observed climate data is considered as the best available estimate of current-day
climate conditions. Hence, observed historic S_r estimates are applied in model simulations and modelled future S_r values
are scaled accordingly. Hence, for every used Regional Climate Model (RCM) and emission scenario (RCP), the 'bias' in
simulated historic storage deficits are subtracted from future storage deficit, derived with RCM simulations.

$$S_{r,cor,fut,min} = S_{r,obs,min} + \Delta(S_{r,mod,fut,min} - S_{r,mod,past,min}) \tag{1}$$
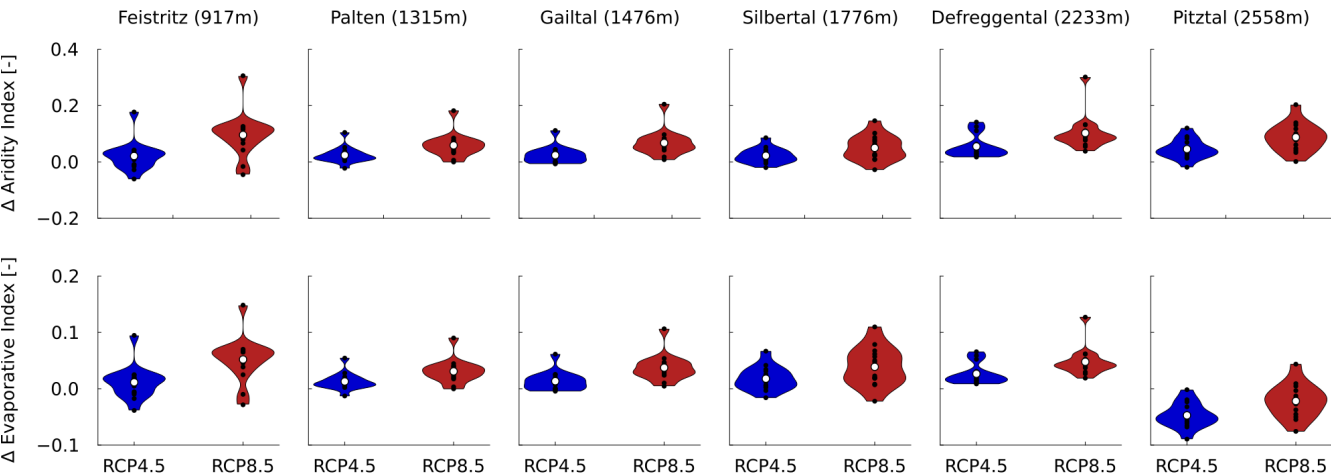
S4 Budyko Framework

Fig. S 4. The mean changes in Aridity and Evaporative Index of the study catchments in the past and under two emission scenarios at the end of the 21st century, using 14 climate model.

Catchment	$\frac{\overline{E_P}}{P_{obs}}$	$\frac{\overline{E_A}}{P_{obs}}$	ω	$\frac{\overline{E_P}}{P_{pro}}$	$\frac{\overline{E_A}}{P_{pro}}$	$1-\frac{\overline{E_A}}{P_{pro}}$	$\overline{Q_{proj}}$
Defreggental	0.418	0.294	1.72	0.449	0.310	0.690	1.829
Feistritztal	0.691	0.593	3.025	0.699	0.598	0.402	0.993
Gailtal	0.368	0.284	1.834	0.369	0.285	0.715	2.699
Paltental	0.425	0.319	1.851	0.447	0.331	0.669	2.271
Pitztal	0.408	0.420	3.863	0.421	0.424	0.588	1.537
Silbertal	0.329	0.302	2.445	0.335	0.307	0.692	2.935

Tab. S 2. Derivation of catchment specific parameter ω from observed aridity and evaporative indices Subsequent calculation of aridity and evaporative indices, runoff coefficients and long term runoff estimates are illustrates for all catchments, one emission scenario and one climate model.
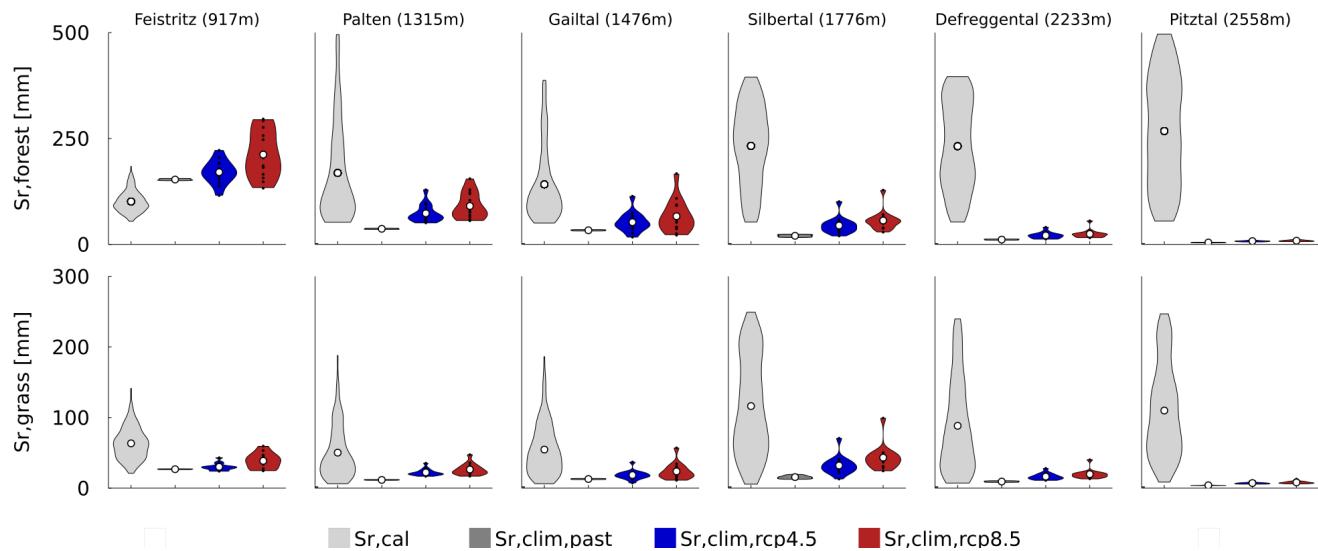
S5 $S_{r,D}$ parameter ranges

Fig. S 5. Parameter ranges obtained from calibration (light grey) and from the water-balance method, using observed climate data (300 parameter sets, grey) and for 14 different RCMs using RCP4.5 (3000 parameter sets, red) and RCP 8.5 (3000, blue)
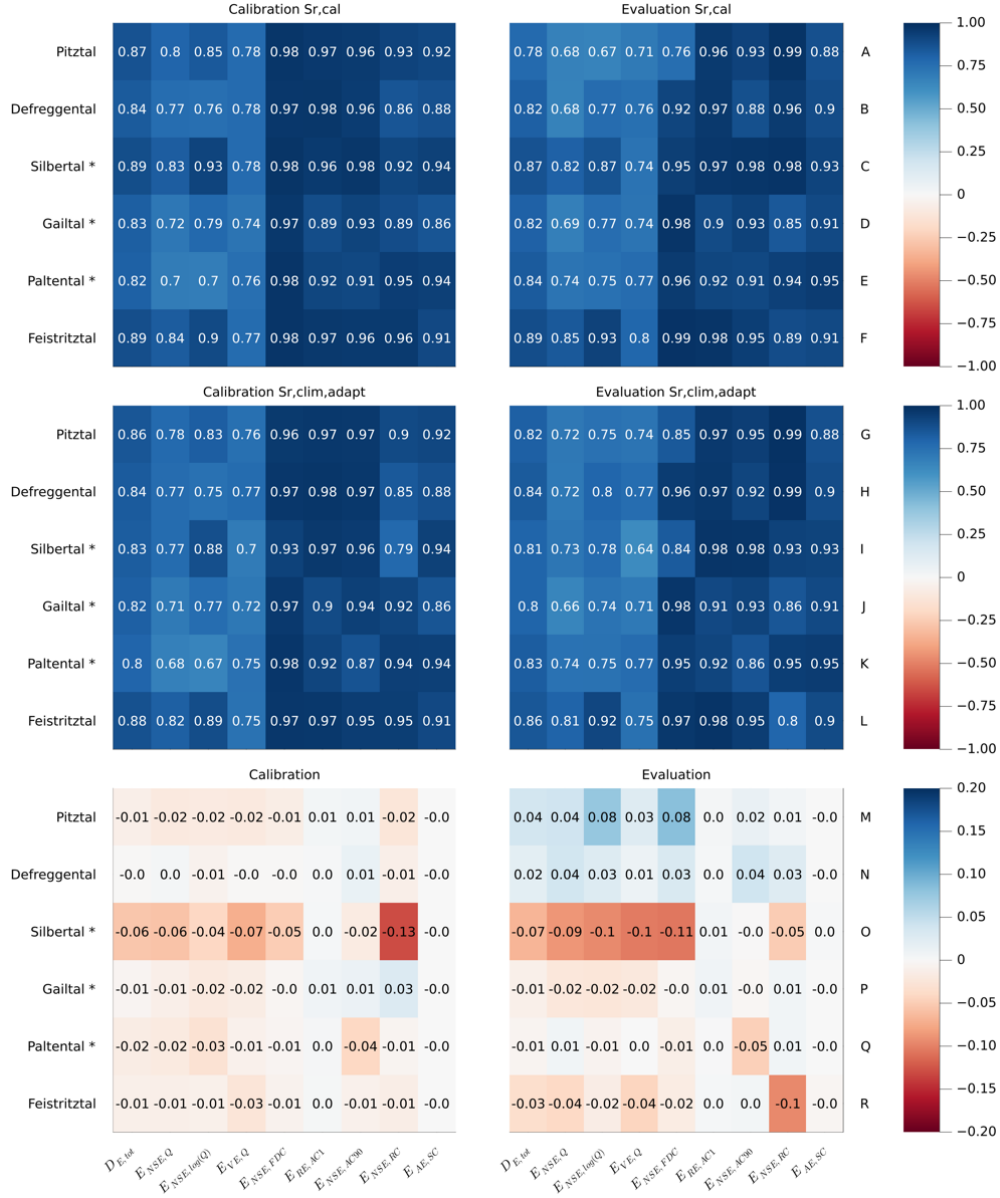
S6 Calibration & Evaluation

Fig. S 6. Model performance of calibrated (row A-F) and 3000 climate-based models (row G-L) during calibration (left) and evaluation (right), for the overall model fit ($D_{E,tot}$) and eight objective functions. Row M-R indicate the difference in performance of climate-based and calibration model, whereas $\Delta D_{E,tot} = D_{E,clim,tot} - D_{E,cal,tot}$. Hence, positive values indicate a better performance of climate-based model. Catchments marked with an aterisk (*) use an 8-year evaluation period instead of 10 years.
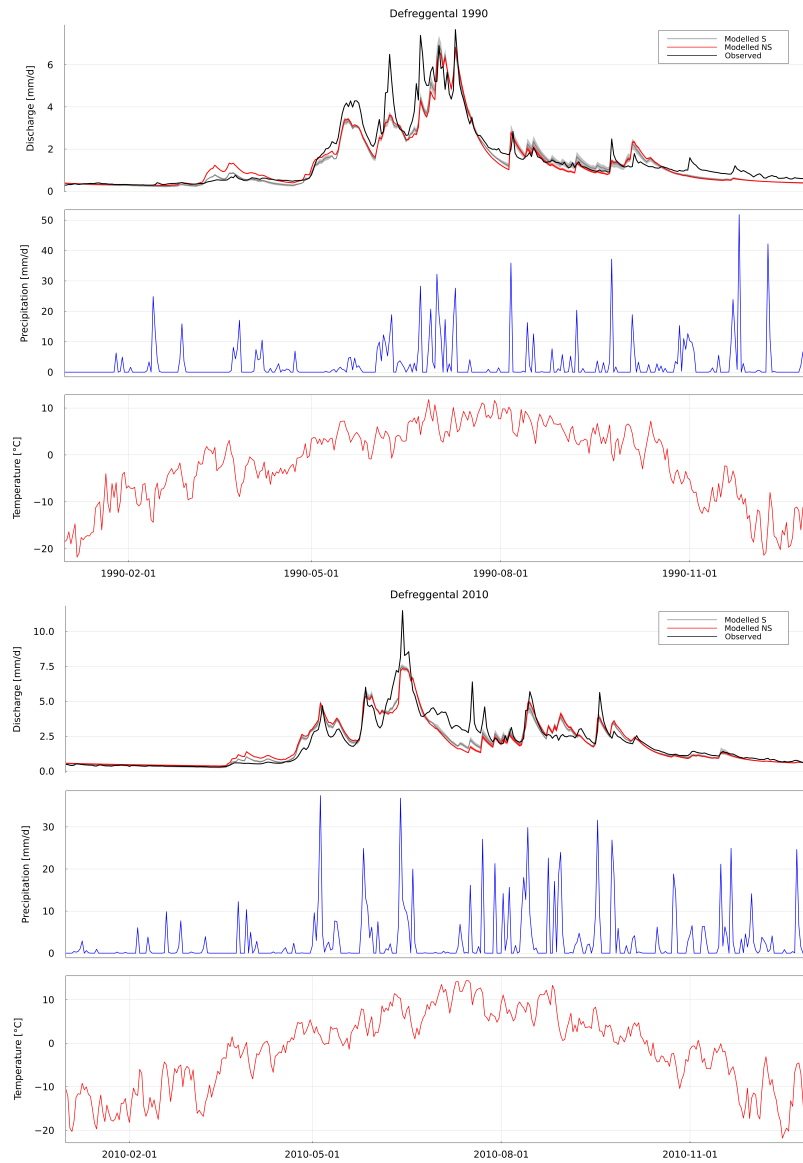
Fig. S 7. Comparison of measured and both calibrated and climate-based modelled runoff in the Defreggental, also showing the corresponding temperature and precipitation. The solid lines indicate mean modelled runoff using the best parameter sets, shaded areas show the range of best parameter sets
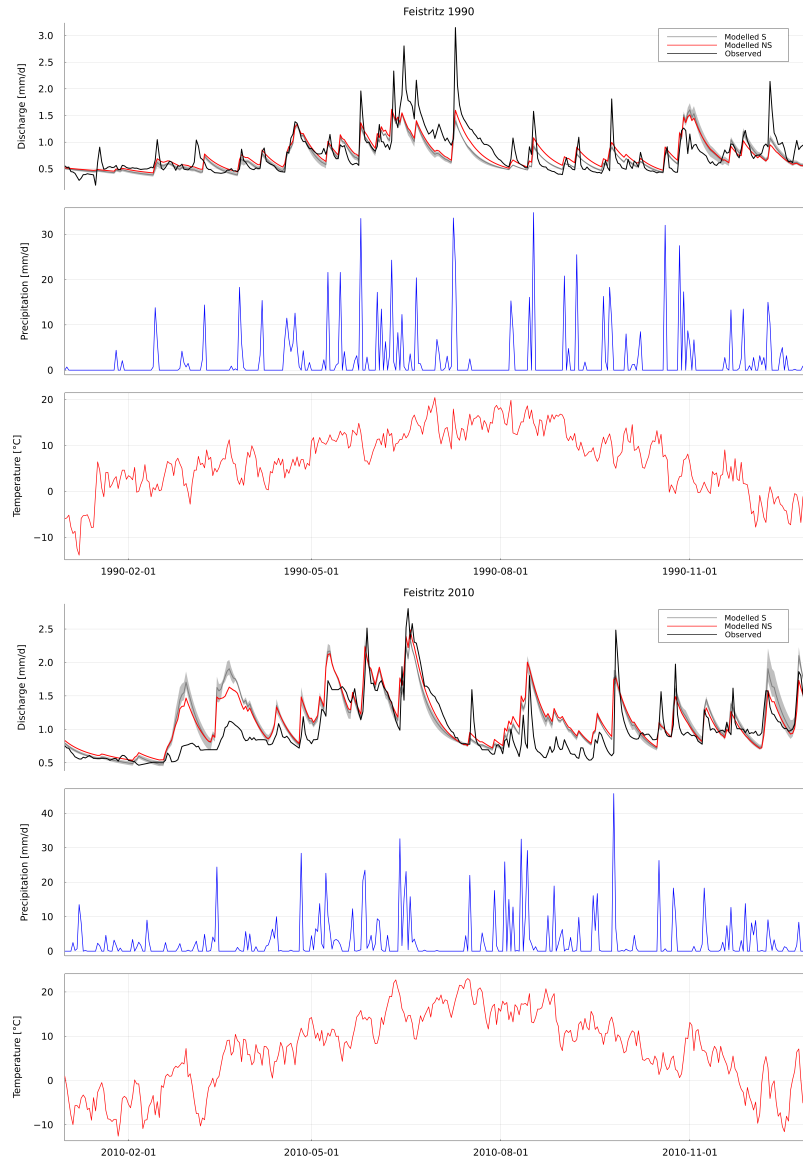
9

Fig. S 8. Comparison of measured and both calibrated and climate-based modelled runoff in the Feistritztal, also showing the corresponding temperature and precipitation. The solid lines indicate mean modelled runoff using the best parameter sets, shaded areas show the range of best parameter sets
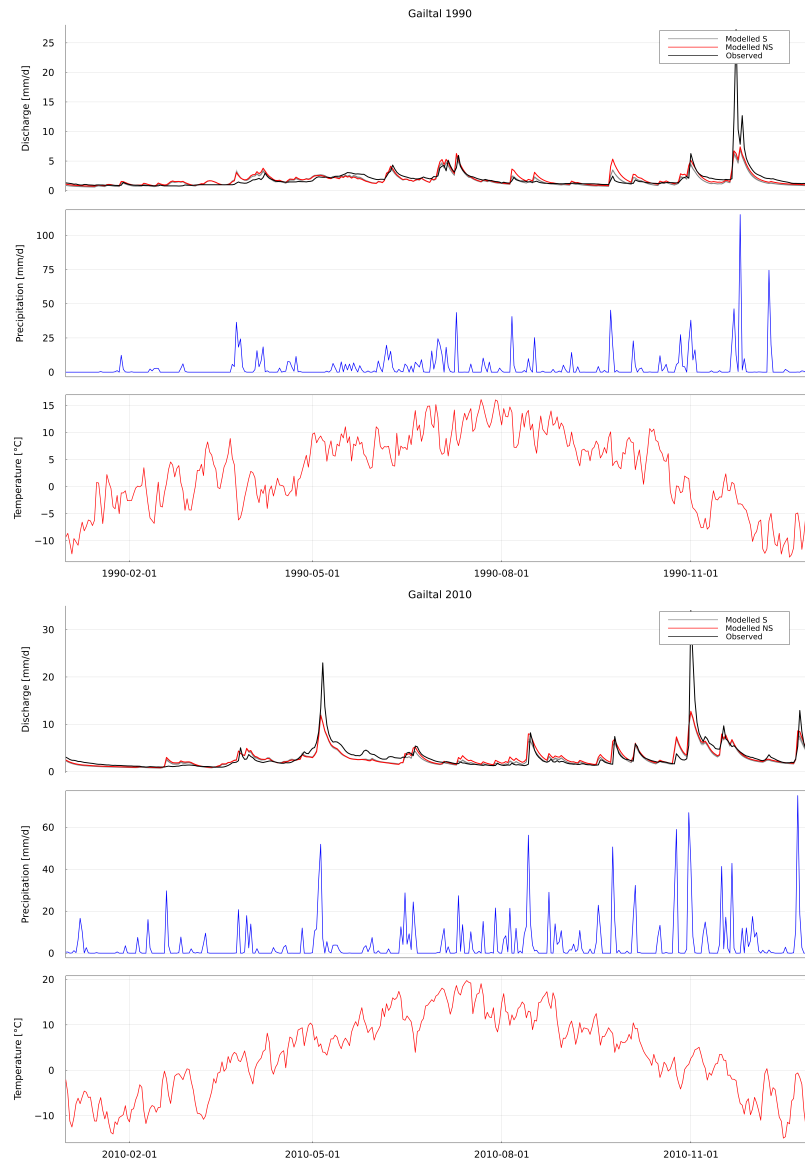
Fig. S 9. Comparison of measured and both calibrated and climate-based modelled runoff in the Gailtal, also showing the corresponding temperature and precipitation. The solid lines indicate mean modelled runoff using the best parameter sets, shaded areas show the range of best parameter sets
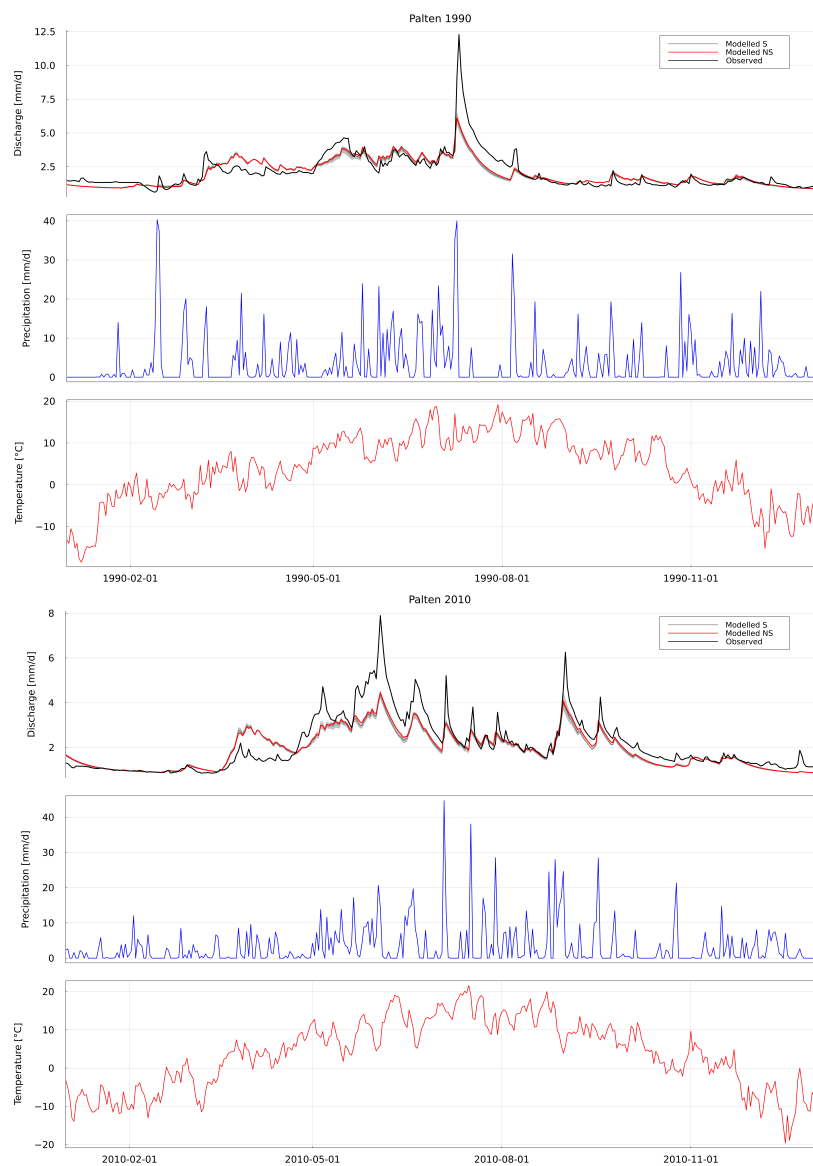
11

Fig. S 10. Comparison of measured and both calibrated and climate-based modelled runoff in the Paltental, also showing the corresponding temperature and precipitation. The solid lines indicate mean modelled runoff using the best parameter sets, shaded areas show the range of best parameter sets

12

Fig. S 11. Comparison of measured and both calibrated and climate-based modelled runoff in the Pitztal, also showing the corresponding temperature and precipitation. The solid lines indicate mean modelled runoff using the best parameter sets, shaded areas show the range of best parameter sets

Tab. S 3. Simulation mean occurance of average timing of AMF over 30years,±1 std, dates refer to mean date in the past

	Model	Past	Date	RCP 4.5	RCP 8.5	Change RCP 4.5	Change RCP 8.5
Feistritztal	clim,stat	162±10	June 11	163±15	145±30	+1 days	-17days
Feistritztal	clim,adapt	162±10	June 11	165±15	151±26	+3 days	-11days
Paltental	clim,stat	174±9	June 23.	173±19	168±26	-1 days	-6 days
Paltental	clim,adapt	174±9	June 23.	167±20	151±25	-7 days	-23 days
Gailtal	clim,stat	273±22	September 30.	294±15	308±17	+21 days	+35 days
Gailtal	clim,adapt	273±21	September 30.	296±19	307±47	+23 days	+34 days
Silbertal	clim,stat	193±9	July 11.	177±11	170±16	-16 days	-23 days
Silbertal	clim,adapt	193±9	July 11.	174±13	162±19	-19 days	-31 days
Defreggental	clim,stat	196±10	July 14.	191±16	198±20	-5 days	+2 days
Defreggental	clim,adapt	196±10	July 14.	188±16	193±21	-8 days	-3 days
Pitztal	clim,stat	189±7	July 7.	179±11	175±14	-10 days	-14 days
Pitztal	clim,adapt	189±7	July 7.	177±11	172±14	-12 days	-17 days

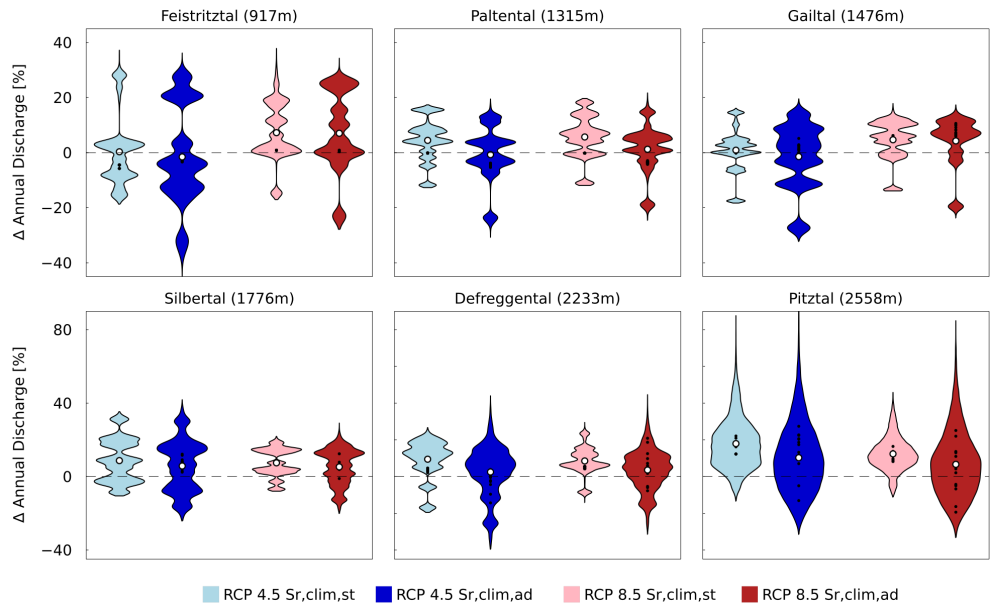35   **S7   Modelled future streamflow**

Fig. S 12. Absolute changes in mean annual discharge for all catchments, using both $S_{r,clim,stat}$ (light) and $S_{r,clim,adapt}$ (dark), for all 14 climate simulations and RCPs. RCP 4.5 is coloured in red and RCP 8.5 in blue.
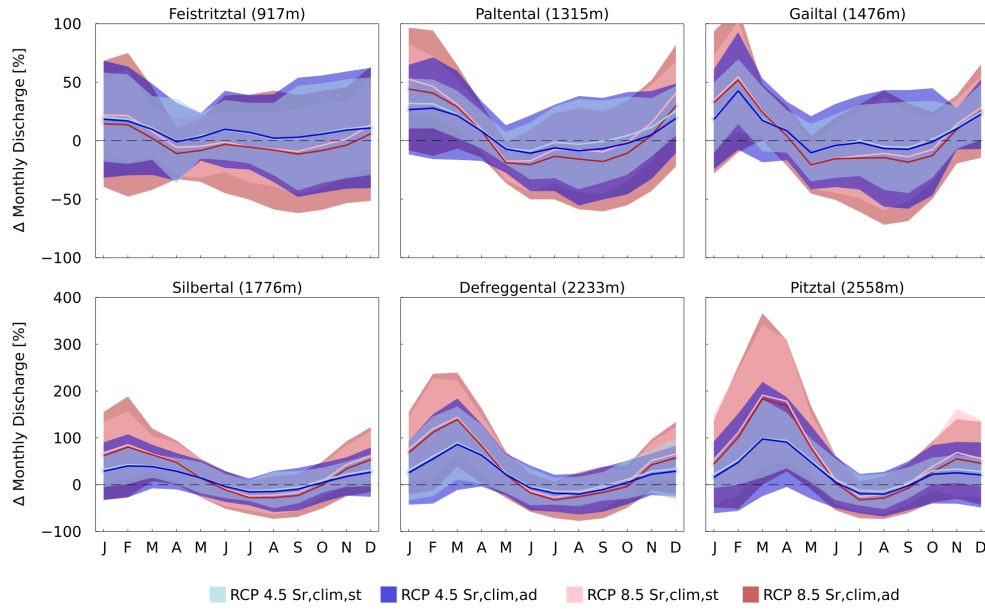
Fig. S 13. Relative changes in mean monthly discharge, for 14 climate scenarios and 2 RCPs, using the climate-based stationary and adaptive model. Results obtained from models featuring $S_{r,clim,stat}$ and $S_{r,clim,stat}$ are respectively depicted in pink and red for RCP 4.5 and lightblue and blue for RCP 8.5.
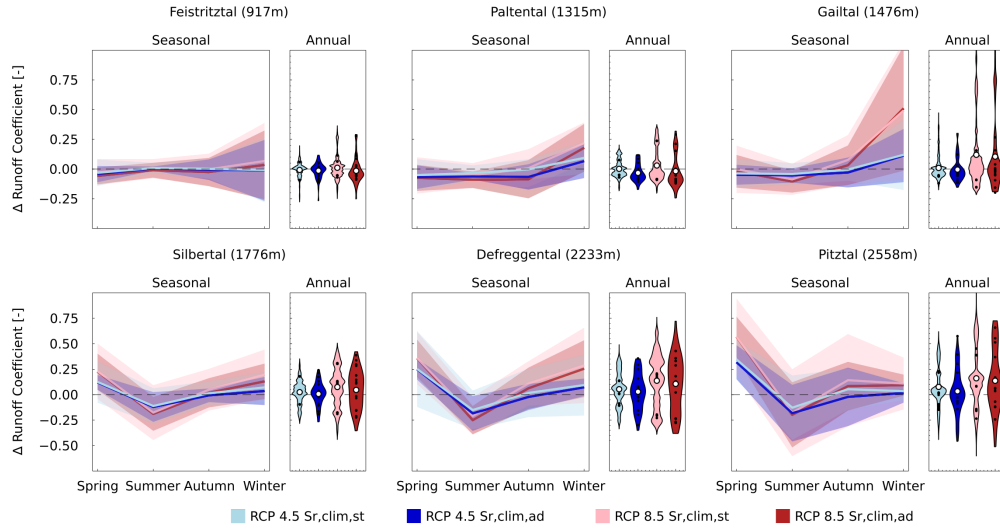

Fig. S 14. Relative changes in 30 years average seasonal runoff coefficient, for 14 climate scenarios and 2 RCPs, using the climate-based stationary and adaptive model. Results obtained from models featuring $S_{r,clim,stat}$ and $S_{r,clim,stat}$ are respectively depicted in pink and red for RCP 4.5 and light blue and blue for RCP 8.5.
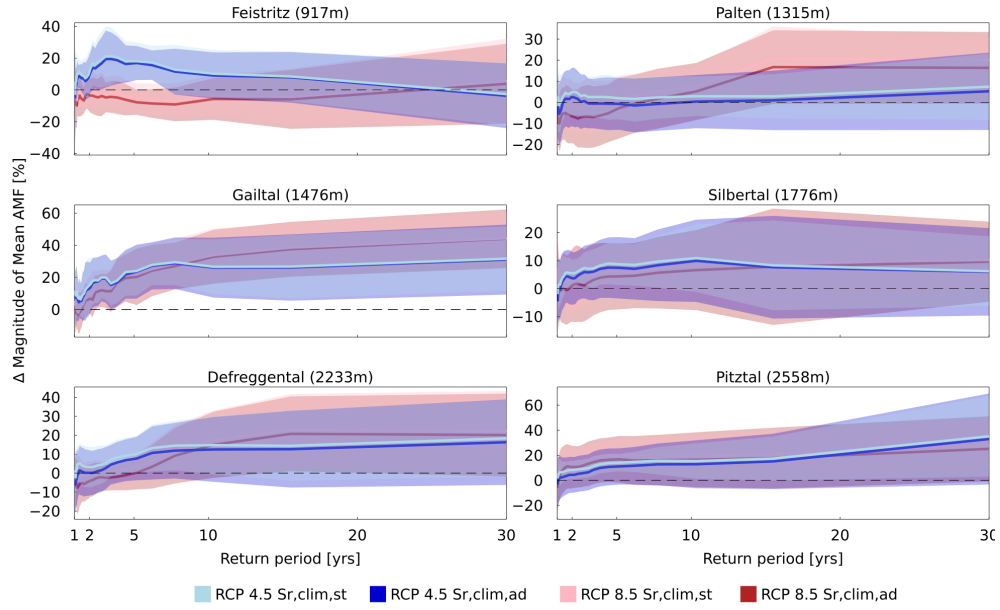
Fig. S 15. Simulated mean relative change in magnitudes of AMF in relation to the return period, for 14 climate scenarios and 2 RCPs, using the climate-based stationary and adaptive model. Results obtained from models featuring $S_{r,clim,stat}$ and $S_{r,clim,stat}$ are respectively depicted in pink and red for RCP 4.5 and light blue and blue for RCP 8.5. Uncertainty bands of 1 std are shaded and mean lines are used to allow for better visualisation. Note the difference in scale for the Gailtal.
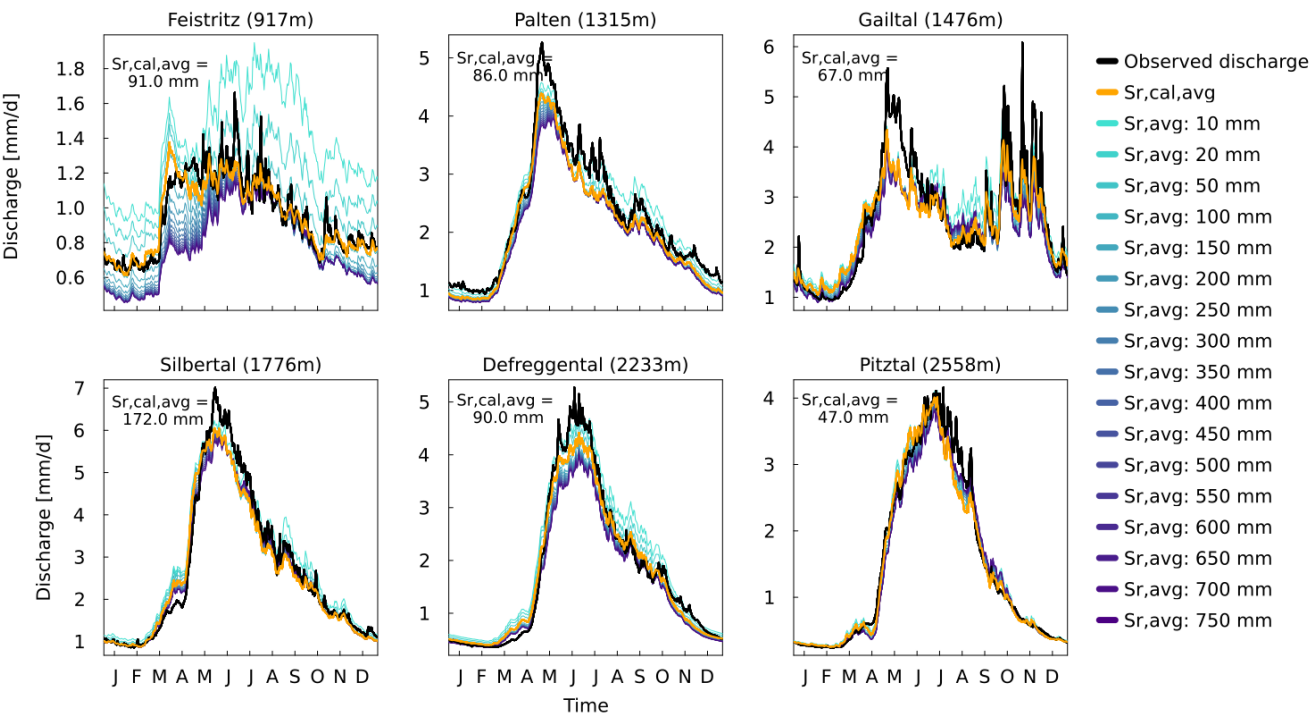
S8   Sensitivity Analysis

Fig. S 16. Sensitivity analysis of the HBV model during the sensitivity period (Pitztal: 1985–2007; Gailtal: 1985–2010; other catchments: 1985-2012). The plots show observed discharge and mean regime curves for different catchment-average storage capacities, averaged across vegetation types.
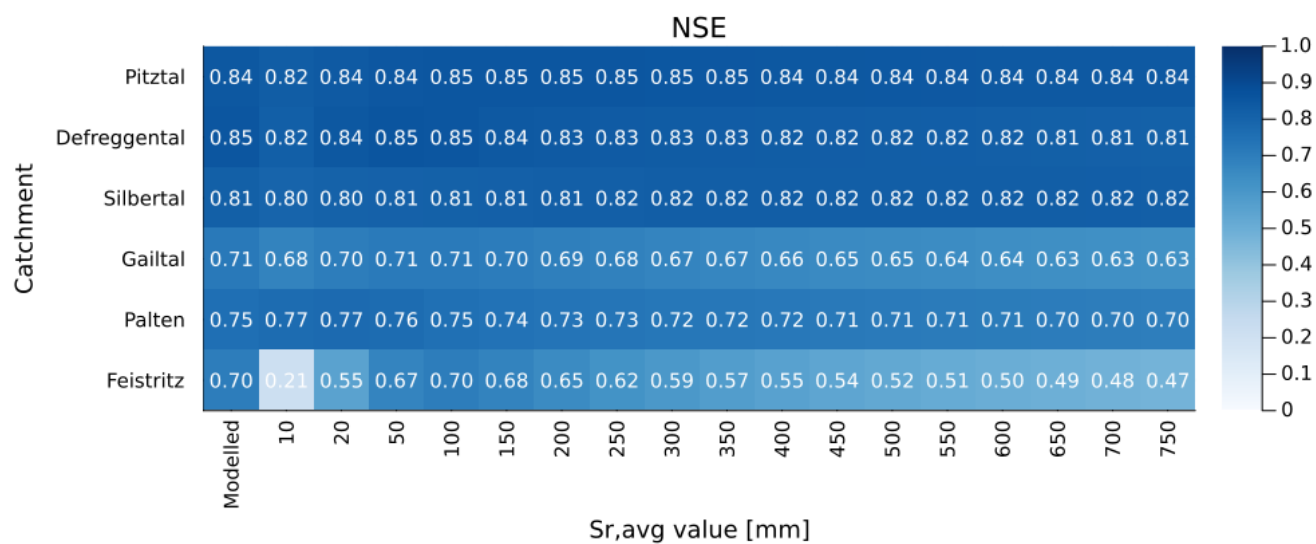
Fig. S 17. Sensitivity analysis of the HBV model during the sensitivity period (Pitztal: 1985–2007; Gailtal: 1985–2010; other catchments: 1985-2012). The heatmap shows relative model performance (NSE) for varying average S_R values and catchment-average storage capacities, averaged across vegetation types.

References

Bouaziz, L., Aalbers, E. E., Weerts, A. H., Hegnauer, M., Buiteveld, H., Lammersen, R., Stam, J., Sprokkereef, E., Savenije, H. H. G., and Hrachowitz, M.: The importance of ecosystem adaptation on hydrological model predictions in response to climate change, Hydrol. Earth Syst. Sci. Discuss., 2021, 1–39, https://hess.copernicus.org/preprints/hess-2021-204/%0Ahttps://hess.copernicus.org/preprints/hess-2021-204/hess-2021-204.pdf, 2021.

Ehret, U., Zehe, E., Wulfmeyer, V., Warrach-Sagi, K., and Liebert, J.: HESS Opinions "should we apply bias correction to global and regional climate model data?", Hydrology and Earth System Sciences, 16, 3391–3404, https://doi.org/10.5194/hess-16-3391-2012, 2012.

Hanus, S.: Effects of Climate Change on Runoff Dynamics in Alpine Catchments, p. 45, 2020.

40